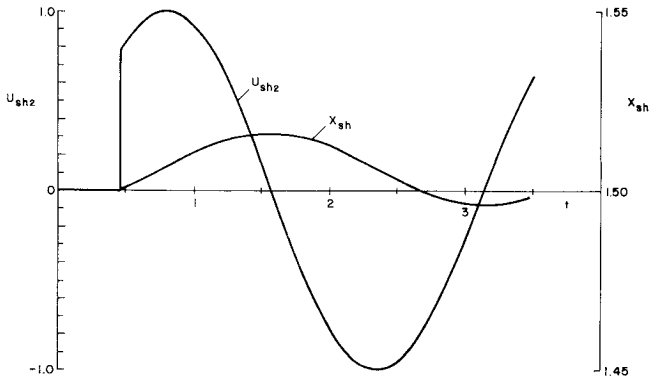

Fig. 3 Shock velocity U_{sh} and position X_{sh} vs time.

Conclusions

This analysis gives a qualitative insight on the nature of unsteady transonic nozzle flow without resorting to the more complicated numerical solutions of transport equations. It was done employing the same technique Richey and Adamson[1] applied to channel flows, and it also can be used to study two-dimension asymmetric flows. It should be noted that this approach is for flows across nozzles displaying a smooth change in cross section. Further, the applied perturbation should not possess a very high frequency since the adopted solution deals with slow time variation regimes. This leads to the choice of a characteristic time of the order of 10^{-2}–10^{-3} s.

References

[1]Richey, G. K. and Adamson, T. C., Jr., "Analysis of Unsteady Transonic Channel Flow with Shock Waves," *AIAA Journal*, Vol. 14, Aug. 1976, pp. 1054–1061.

[2]Sichel, M., "The Effect of Longitudinal Viscosity on the Flow at a Nozzle Throat," *Journal of Fluid Mechanics*, Vol. 25, 1966, pp. 769–786.

[3]Adamson, T. C., Jr., Messiter, A. F., and Richey, G. K., "On the Matching of Solutions for Unsteady Transonic Nozzle Flows," *Archiwum Mechaniki Stosowanej*, Vol. 26, 1974, pp. 617–628.

[4]Messiter, A. F. and Adamson, T. C., Jr., "On the Flow Near a Weak Shock Wave Downstream of a Nozzle Throat," *Journal of Fluid Mechanics*, Vol. 60, 1975, pp. 97–108.

[5]Adamson, T. C., Jr., Messiter, A. F., and Liou, M. S., "Large Amplitude Shock-Wave Motion in Two-Dimensional, Transonic Channel Flows," *AIAA Journal*, Vol. 16, Dec. 1978, pp. 1240–1247.

[6]Lin, C. Q. and Shen, S. F., "Two-Dimensional Transonic Nozzle Flows with Shock," *AIAA Journal*, Vol. 19, Nov. 1981, pp. 1494–1496.

Finite-Element Method Applied to Transonic Flow Over a Bulbous Payload Shroud

R. C. Mehta* and T. Jayachandran†
Vikram Sarabhai Space Centre, Trivandrum, India

Introduction

ANALYSIS of transonic flow over a bulbous payload shroud of a launch vehicle requires accurate modeling of the shock boundaries as well as the details of the subsonic and supersonic regions and shock. A numerical analysis is also needed to complement wind-tunnel tests, when tunnel-wall interference may induce large deviations from free-air conditions even for very small blockage ratios. The efficiency of the numerical approach in analyzing the bulbous shape geometrical configuration is directly related to the applicability of irregular computational grids.

Numerical solution of steady, inviscid, and axisymmetric transonic flow over blunt and boat-tail configurations has been obtained using the finite-difference method by several researchers[1–4] during the last few years. During these investigations, the importance of computational grid, effect of artificial viscosity, and relaxation factor in the computation of transonic flow was observed. Application of the finite-element method for the analysis of two-dimensional inviscid transonic flow problem has been considered by several investigators.[5–7] One of the main advantages of the finite-element approach has been practicability of setting an irregular computational grid to fit a particular flow problem. This property therefore proves to be important for the solution of transonic flow over a bulbous payload shroud of a typical launch vehicle. The finite-element method has been applied by Chima and Gerhart[8] to the solution of subsonic flow over a boat-tail body.

The present work uses a mesh of triangular finite elements. This is chosen because it enables a large number of small elements to be packed into the regions of greatest interest such as in the vicinity of blunt body and boat-tail regions. The importance of designing a computational grid suitable for both subsonic regions and supersonic pockets to obtain accurate and efficient solution has been investigated in the present analysis. A shock-capturing technique is employed in conjunction with the pseudotime integration scheme.[9] The choice of artificial viscosity, relaxation factors, and design of a computational grid is investigated. It will be demonstrated that the finite-element method is a practical and efficient tool in treating complex flow problems. Comparisons between analysis and experiment have been made for two different types of axisymmetric geometry of bulbous payload shroud.

Full Potential Equations

The full potential equation for steady, inviscid, and irrotational flow in a conservation form for an axisymmetric body can be written as

$$(\rho r \phi_{,r})_{,r} + (\rho r \phi_{,z})_{,z} = 0 \qquad \text{on } v \tag{1}$$

where ϕ is the velocity potential, v the solution domain, and ρ the mass density of the fluid. Since no entropy can be created in irrotational flow, the density can be computed using the isentropic relation. Equation (1) is second-order quasilinear of elliptic type in subsonic, parabolic type in sonic, and hyperbolic type in supersonic points of flow.

The boundary condition at the solid surface is that the velocity normal to the surface equal to zero. At the downstream boundary of the computational field, the potential function ϕ is specified. The boundary conditions on the far field on an isolated bulbous payload shroud or body are only approximate. The correct boundary condition is that the velocities approach to freestream values far from the body. This boundary condition cannot be satisfied directly for a potential flow solution in a finite computational domain. The present far-field boundary conditions are satisfactory provided the boundaries are located far enough from the body. Locating the far-field boundaries 10–12 maximum body diameters away from the body is usually sufficient to insure minor effect of the boundary condition on the computed flowfield near the body. If the far-field boundary is so placed, the effect of the boundary conditions are small and are of the order of or smaller than other approximations such as treating a bulbous

Received Nov. 19, 1987; revision received July 20, 1988.

*Engineer, Aerodynamics Division.
†Engineer, Propulsion Engineering Division.

payload shroud as an isolated body. The general boundary conditions of Eq. (1) can be mathematically written as

$$\phi = \phi_0 \qquad \text{on } S_1 \tag{2}$$

$$\rho\phi_{,n} = f \qquad \text{on } S_2 \tag{3}$$

where ϕ_0 and f are some specified quantities on the boundary $S = S_1 + S_2$ and n is the outward normal on S_2.

Finite-Element Formulation

The Bateman's variational formulation[9] is employed for a finite-element formulation of Eqs. (1-3). A discretization in terms of finite element is introduced to solve the full potential equation. The interpolation can be expressed for each element as

$$\phi^e(r,z) = N^T\phi^e \tag{4}$$

where ϕ^e are the nodal values of the velocity potential, and N is the shape function. Following the standard finite-element formulation, a system of nonlinear algebraic equations is obtained in terms of the nodal velocity potential as

$$K\phi = f \tag{5}$$

where

$$K = \sum_e \int \rho_e r(N_{,r}N^T_{,r} + N_{,z}N^T_{,z})\, dv$$

$$f = \sum_e \int_{S_2^e} f_e N\, dS$$

$$\phi = \sum_e \phi^e$$

The solution of these nonlinear equatons is obtained using pseudounsteady formulation as

$$\Delta t C\dot{\phi} + K\phi = f \tag{6}$$

where Δt is a pseudotime increment, and $C = (K/\omega)$ is the damping matrix of Eq. (16). Here ω is a relaxation factor. Using a standard backward-differencing scheme, Eq. (16) is obtained as

$$K^{n+1}\bar{\phi}^{n+1} = f^{n+1} \tag{7}$$

with

$$\phi^{n+1} = \omega\bar{\phi}^{n+1} + (1-\omega)\phi^n \tag{8}$$

where n is the pseudotime step. The value of $\omega = 0.8$–1.2 is selected in the present analysis. An IMSL subroutine LEQ1PB is called to solve the matrix equations. Once each value of ϕ in the field has converged to within a specified tolerance, the matrix iteration is stopped.

The natural procedure of substituting $\rho_e^{n+1} \approx \rho_e^n$ is entirely satisfactory in subsonic flow in evaluating K^{n+1} at time step n. But in the supersonic flow, the process becomes numerically unstable, and if there is a patch of supersonic flow covering more than a very few elements, the results are totally unrealistic. In order to overcome this problem, use is made of "upwind densities." For sufficiently streamlined elements and uniform grids, ρ_e^{n+1} can be computed as follows

$$\rho_e^{n+1} \approx \alpha_e\rho_{eu}^n + (1-\alpha_e)\rho_e^n \tag{9}$$

where ρ_{eu} is the mass density of the nearest element at the upstream side of e, and α_e is the artificial viscosity coefficient for the element.

The role of artificial viscosity is to enable the use of the finite-element method to solve a mixed elliptic/hyperbolic problem. It performs this feat by adding dissipation into the differential equation or equivalently by biasing the scheme in the upstream direction. The amount of artificial viscosity required for convergence of the pseudotime integration scheme depends on the local Mach number as well as the computational grid and the distribution of the error in the initial solution. One of the most important factors in obtaining the efficiency of the solution procedure has been the choice of the artificial viscosity distribution. Various types of artificial viscosity-coefficient expressions[10-12] were tested in the program, and the following relationship[13] for α_e is selected:

$$\alpha_e = 0.3 + (1 - 1/M_e^2) \qquad M_e \geq 1$$

$$\alpha_e = 0.3\, M_e^7 \exp\,[-20(M_e - 1)^2] \qquad M_e < 1 \tag{10}$$

where M_e is element Mach number. Equation (10) gives continuity of α_e and $d\alpha_e/dM_e$ at $M_e = 1.0$. Numerical results con-

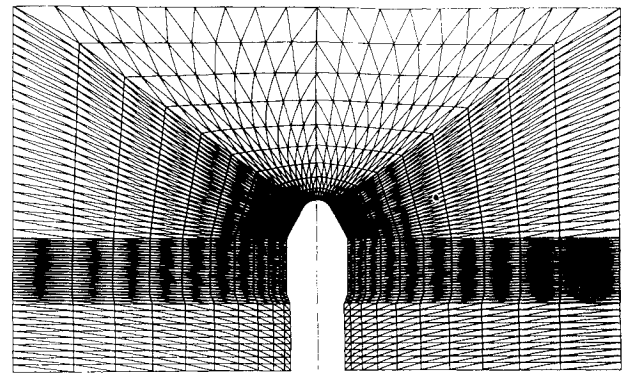

Fig. 1 Computational grid for M11.

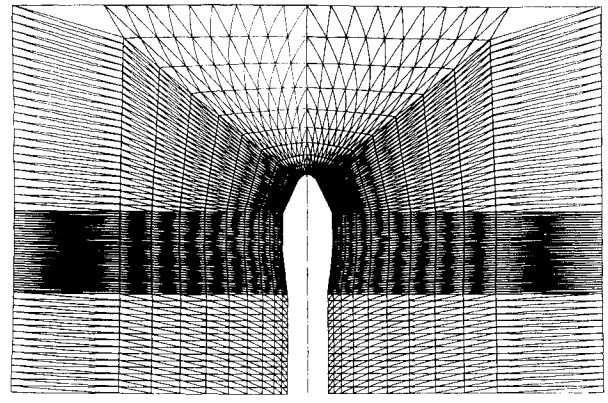

Fig. 2 Computational grid for M12.

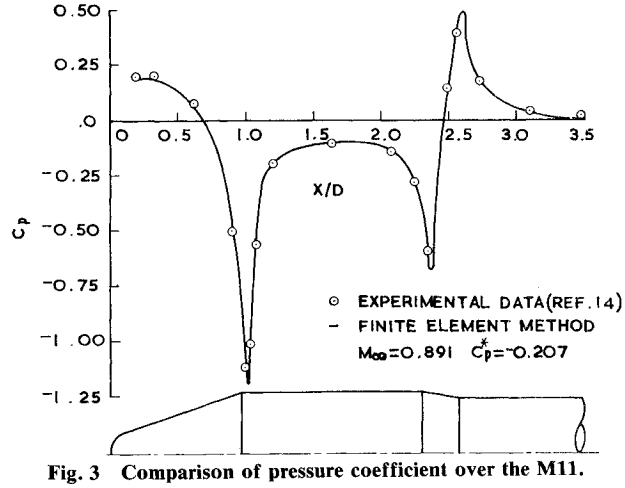

Fig. 3 Comparison of pressure coefficient over the M11.

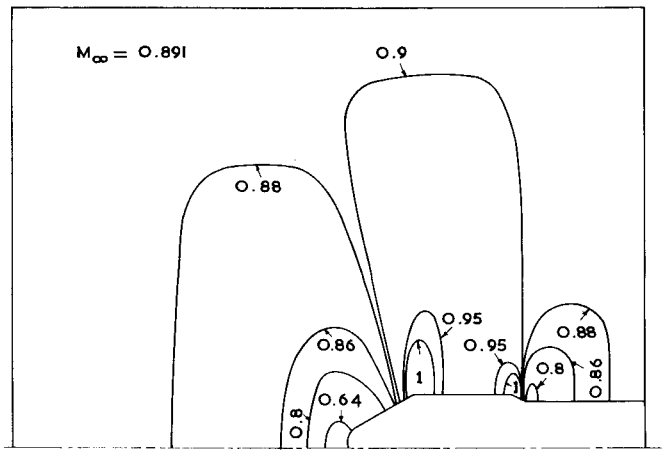

Fig. 4 Iso-mach lines for M11 configuration.

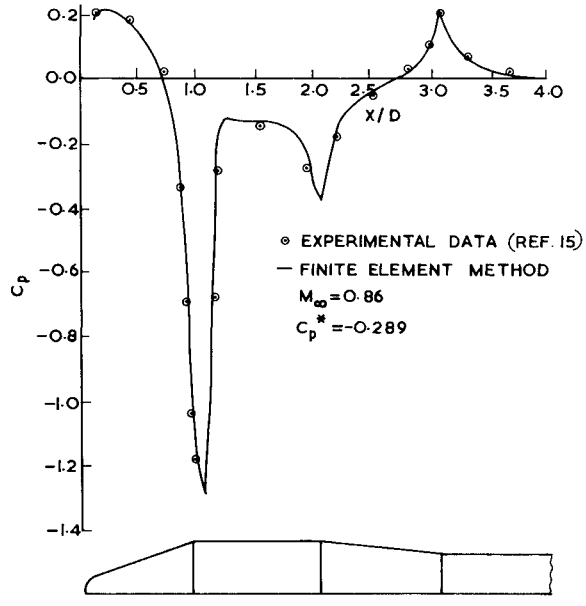

Fig. 5 Comparison of pressure coefficient over the M12.

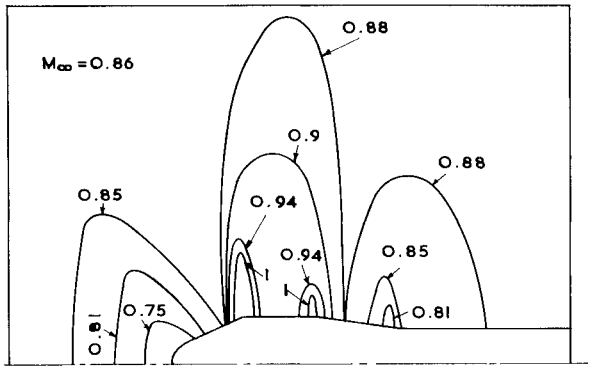

Fig. 6 Iso-mach lines for M12 configuration.

firmed that Eq. (10) is a satisfactory choice of α_e for a wide range of transonic flows. In order to enhance the convergence of the numerical scheme, a large value of α_e is used initially, which is gradually refined to the value of Eq. (10) as convergence is approached.

A shock-capturing technique is used in the present analysis. Shocks are free to develop at the element interfaces as discontinuities in the mass flux. This can occur only when an upwinding is used for a supersonic element neighboring a subsonic element. Because of the convective nature of the flow, compression shocks are produced automatically.

Results

The primary objective of this work was the development of an accurate, computationally efficient method for solving the full potential equation over a bulbous payload shroud. The geometrical configuration consists of a blunt nosecone cylinder-flare cylinder. To assess the accuracy of the method, comparisons of numerical results with experiment are presented for two different types of axisymmetric bodies. Figures 1 and 2 depict the discretization of the computational domain using finite triangular elements.

The first comparison between theory and experiment[14] is for an axisymmetric model tested in a transonic wind tunnel. Figure 3 presented the pressure distribution C_p at a freestream Mach number of 0.89. The body shape is shown schematically below the figure. The body length is nondimensionalized with respect to maximum body diameter. The finite-element method took 55 iterations, 348 s of CPU time, and 67 K of memory of a CDC 170/730 computer to obtain a converged solution. The comparison between numerical results and experiment is excellent. It reveals that the program appears to be accurate for predicting an inviscid flowfield. Figure 4 shows the computed Mach number contours.

The second comparison between theory and experiment[15] is done on another bulbous payload shroud at a freestream Mach number of 0.86. In this example, the program took 50 iterations, 368 s of CPU time, and 69 K of storage capacity of a CDC 170/730 computer to get a converged solution. Figures 5 and 6 show the variation of pressure coefficient and iso-Mach lines, respectively. Overall agreement with experiment is found to be good. Two regions of embedded supersonic flow are quite evident, and both are predicted by the theory as it can be seen in Fig. 6.

Conclusions

The capability, speed, and accuracy of the computational procedures in this investigation are demonstrated by numerical examples that are compared with experiment. The finite-element method for the governing equation and the resulting computational procedure eliminates many of the difficult problems associated with numerical analysis of fluid flow. The correlation between theory and experiment is good considering the possibilities of wind-tunnel interference and viscous effects. The computer program is simple and involves no complicated numerical scheme.

References

[1]Krupp, J. A. and Murman, E. M., "Computation of Transonic Flows Past Lifting Bodies and Slender Bodies," *AIAA Journal*, Vol. 10, July 1972, pp. 880–886.

[2]South, C. J., Jr. and Jameson, A., "Relaxation Solution for Inviscid Axisymmetric Transonic Flow Over Blunt or Pointed Bodies," *Proceedings of the AIAA Computational Fluid Dynamics Conference*, AIAA, New York, July 1973, pp. 8–17.

[3]Purvis, J. W. and Burkhalter, J. E., "Prediction of Critical Mach Number for Store Configurations," *AIAA Journal*, Vol. 17, Nov. 1979, p. 1170.

[4]Chow, W. L., Bober, L. J., and Anderson, B. H., "Numerical Calculation of Transonic Boattail Flow," NASA TND 7984, June 1975.

[5]Akay, H. U. and Ecer, A., "Transonic Flow Computation in Cascades Using Finite-Element Methods," *Journal of Engineering and Power*, Vol. 103, Oct. 1981, pp. 657–664.

[6]Deconinck, H. and Hirsch, Ch., "Finite-Element Methods for Transonic Blade-to-Blade Calculation in Turbomachines," *Journal of Engineering for Power*, Vol. 103, Oct. 1981, pp. 665–677.

[7]Deconick, H. and Hirsch, Ch., "Subsonic and Transonic Calculation of Cascade Flow," *Computing Methods in Applied Sciences and Engineering*, edited by R. Glowiniski and J. L. Lions, North-Holland, Amsterdam, 1980, pp. 175–195.

[8]Chima, R. V. and Gerhart, P. M., "Finite-Element Analysis of Inviscid Subsonic Boattail Flow," *AIAA Journal*, Vol. 20, Feb. 1982,

pp. 190–195.
[9]Ecer, A. and Akay, H. U., "Finite-Element Analysis of Transonic Flows in Cascades – Importance of Computational Grids in Improving Accuracy and Convergence," NASA CR-3446, July 1981.
[10]Deconinck, H. and Hirsch, Ch., "Transonic Flow Calculations with Finite Elements," *GAMM Workshop on Transonic Flow Calculations with Shocks*, Vieweg, 1979.
[11]Hafez, M., South, J., and, Murman, E., "Artificial Compressibility Methods for Numerical Solutions of Transonic Full Potential Equations," *AIAA Journal*, Vol. 17, Aug. 1979, pp. 838–844.
[12]Akay, H. U. and Ecer, A., "Finite-Element Analysis of Transonic Flows in Highly Staggered Cascades," AIAA Paper 81-0210, Jan. 1981.
[13]Whitehead, D. S. and Newton, S. G., "Finite-Element Method for the Solution of Two-Dimensional Transonic Flows in Cascades," *International Journal of Numerical Methods in Fluids*, Vol. 5, Feb. 1985, pp. 115–132.
[14]Prasad, J. K., Varambally, B. S., Pillai, N. M., and Srivaram Krishnan, A. E., "Aerodynamic Load on Heat Shield in Mach Number Range of 0.8 to 1.1," Vikram Sarakhai Space Centre, Trivandrum, India, EWTT:02:84, June 1984.
[15]Ahmed, S., "Pressure Measurements in the Heat Shield Region at Transonic Speeds," National Aeronautical Laboratory, India, TWT, 1-32-84, July 1984.

Transonic Flow Modes of an Axisymmetric Blunt Body

Keith Koenig*
Mississippi State University, Starkville, Mississippi

David H. Bridges†
California Institute of Technology
Pasadena, California
and
Gary T. Chapman‡
NASA Ames Research Center
Moffett Field, California

Introduction

THE use of induced flow separation devices for blunt-body drag reduction has proved effective in several practical applications. Notable examples are the spike used on the Trident ballistic missile[1] and the various cab-mounted shields found on large tractor-trailer trucks.[2] Little has been done to exploit this concept at transonic speeds, however. The present work is intended partly to provide information on the aerodynamic properties of flow separation devices at transonic speeds in order to assess their potential in this flow regime.

This work has a broader and more fundamental purpose, however, and that is to examine the fluid mechanic properties of a cavitylike flowfield in the transonic regime. The geometry in question is sketched in the inset of Fig. 1. It is composed of a simple, flat-faced, circular cylinder (diameter d_2) aligned with the flow and in front of which is coaxially extended a smaller-diameter flat-faced cylinder, known as the probe. The probe diameter d_1 and length l can be varied. For relatively short probes, there is a single separated zone between the probe face and the cylinder face, whereas longer probes produce two separated zones in this region.[3] These two situations correspond to the open and closed modes, respectively, of a cavity or cutout in a wall[4] (see the inset of Fig. 3). The probe length, which distinguishes the open from the closed mode, is designated as the critical length l_{cr}. Cavitylike flows are encountered in a wide variety of situations, and this study is intended to explore one such situation found in drag reduction schemes.

Presented as Paper 88-3536 at the AIAA 1st National Fluid Dynamics Conference, Cincinnati, OH, July 25-28, 1988; received Aug. 15, 1988; revision received Nov. 11, 1988. This paper is declared a work of the U.S. Government and is not subject to copyright protection in the United States.

*Associate Professor, Aerospace Engineering. Member AIAA
†Graduate Student, Aeronautics. Student Member AIAA.
‡Senior Staff Scientist, Thermosciences Division. Associate Fellow AIAA.

Experimental Details

In this presentation, measurements of drag coefficient C_D as a function of probe length, probe diameter, and freestream Mach number will be used to calculate the flowfield characteristics. The drag coefficient is based on the drag force acting on the entire probe and cylinder minus the cylinder base drag. The reference area is the cylinder cross-sectional area. No corrections for blockage were made to the drag coefficient, and its estimated accuracy is ± 0.02.

These measurements were obtained in the (now nonexistent) 1.83-m × 1.83-m supersonic wind tunnel at the NASA Ames Research Center. The Mach number M ranged from 0.8 to 1.5, and the stagnation temperature and pressure were nominally atmospheric for the majority of the tests. The cylinder had a diameter of 127 mm and was 889 mm long. Three probe diameters were used giving diameter ratios d_1/d_2 of 0.248, 0.368, and 0.45. The smallest probe had a length ratio l/d_2 up to 3; the two larger probes had maximum l/d_2 of 2. The results to follow are representative examples for the smallest probe diameter; a complete presentation for all diameters can be found in Ref. 5.

Results and Discussion

Figure 1 demonstrates how C_D varies with length ratio for fixed Mach number. The trends for subsonic and supersonic flow have qualitative similarities. The value of C_D at very short lengths is large and roughly proportional to the freestream stagnation pressure coefficient. Increasing length brings about a rapid decrease in C_D to a minimum value. The subsonic minimum is broad and is followed by a gradual increase to a plateau. The supersonic flow abruptly changes to a higher drag level; the probe is too short to show the asymptotic behavior. Hysteresis (not unique to this experiment[6]) appears in the supersonic drag as the probe is subsequently shortened; no subsonic hysteresis occurs. The magnitude of the drag reduction due to the probe, as much as two-thirds of the zero length drag, is significant enough to perhaps be of practical value.

Insight into the fluid mechanic properties of this flow system is provided by the alternate presentation of C_D as a

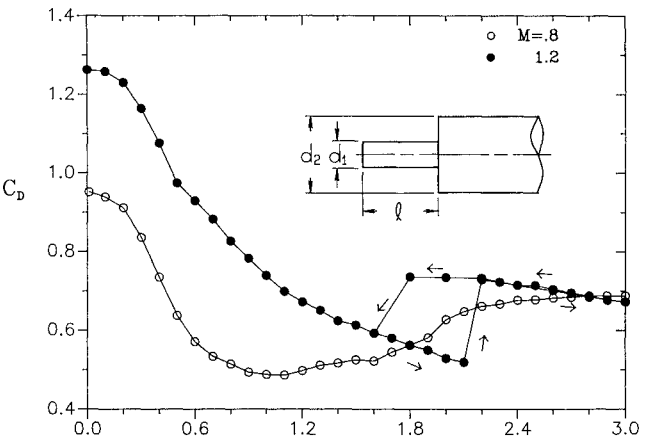

Fig. 1 Influence of probe length on drag coefficient, d_1/d_2 = 0.248.